Field-induced quadrupolar quantum criticality in PrV_{2}Al_{20}

Yasuyuki Shimura, Masaki Tsujimoto, Bin Zeng, Luis Balicas, Akito Sakai, and Satoru Nakatsuji

Phys. Rev. B **91**, 241102 — Published 4 June 2015

DOI: 10.1103/PhysRevB.91.241102

Field-Induced Quadrupolar Quantum Criticality in PrV_2Al_{20}

Yasuyuki Shimura[1],* Masaki Tsujimoto[1], Bin Zeng[2], Luis Balicas[2], Akito Sakai[1,3], and Satoru Nakatsuji[1,4]†
[1]*Institute for Solid State Physics, The University of Tokyo, Kashiwa, Chiba 277-8581, Japan*
[2]*National High Magnetic Field Laboratory (NHMFL), Florida State University, Tallahassee, Florida 32310, USA*
[3]*I. Physikalisches Institut, Georg-August-Universität Göttingen, 37077 Göttingen, Germany*
[4]*PRESTO, Japan Science and Technology Agency (JST), 4-1-8 Honcho Kawaguchi, Saitama 332-0012, Japan*

PrV_2Al_{20} is a heavy fermion superconductor based on the cubic Γ_3 doublet that exhibits nonmagnetic quadrupolar ordering below ~ 0.6 K. Our magnetotransport study on PrV_2Al_{20} reveals field-induced quadrupolar quantum criticality at $\mu_0 H_c \sim 11$ T applied along the [111] direction. Near the critical field $\mu_0 H_c$ required to suppress the quadrupolar state, we find a marked enhancement of the resistivity $\rho(H,T)$, a divergent quasiparticle effective mass and concomitant non-Fermi liquid (NFL) behavior (i.e. $\rho(T) \propto T^n$ with $n \leq 0.5$). We also observe the Shubnikov-de Haas effect above $\mu_0 H_c$, indicating effective mass enhancement or $m^*/m_0 \sim 10$. This reveals the competition between the nonmagnetic Kondo effect and the intersite quadrupolar coupling which leads to pronounced NFL behavior in an extensive region of T and $\mu_0 H$ emerging from the quantum critical point.

PACS numbers: 75.47.-m, 75.25.Dk, 72.15.Qm

Quantum criticality in correlated electron systems has attracted significant attention because of the formation of novel quantum phases such as exotic superconductivity in the vicinity of a quantum critical point (QCP)[1]. Moreover, the breakdown of the standard Fermi-liquid behavior has been seen almost routinely nearby a magnetic QCP in a variety of strongly correlated electron systems, ranging from cuprates, iron pnictides and heavy fermion intermetallics[2,3]. Whether another type of instability such as orbital ordering and its associated orbital fluctuations may drive novel types of metallic state and unconventional superconductivity has been an active area of research[1,4–8]. Experimentally, however, quantum criticality due solely to an orbital origin was never observed in metallic systems.

For the study of quantum criticality, $4f$-electron systems are well suited. These systems provide various archetypical examples due to the availability of high-purity single crystals and the relatively low characteristic energy scales which are highly tunable by disorder-free control parameters such as magnetic field or pressure. To date, among heavy-fermion intermetallics, most of the study on QC was performed on compounds containing either Ce ($4f^1$) or Yb ($4f^{13}$) (see, for example, Refs. 9–13) ions whose crystalline-electric-field (CEF) ground-state is composed of Kramers doublets and therefore is magnetic.

In transition metal systems, the coupling between spins and orbitals is unavoidable and produces various interesting spin-orbital ordered and disordered states[14,15]. In contrast, an f-electron system may provide a nonmagnetic CEF ground-state doublet, where orbitals are the only active degree of freedom. In effect, some Pr ($4f^2$)-based cubic compounds are found to host the Γ_3 non-Kramers ground-state doublet, which has no magnetic moment but carries an electric quadrupole moment. In these systems, due to strong intra-atomic spin-orbit coupling, the total angular momentum J represents the magnetic and orbital states, and in particular, the electric quadrupole moment corresponds to the orbital degree of freedom. A number of cubic $4f^2$ Γ_3 systems were studied and various interesting electric phenomena were experimentally reported including a ferro and antiferro quadrupolar ordering depending on the type of the RKKY-type interaction[16–20]. As a competing effect, a nonmagnetic form of the Kondo effect is proposed that quenches the quadrupole moments[21,22]. Thus, the tuning of these competing effects may lead to quadrupolar QC.

In fact, quadrupolar quantum criticality was suggested by recent experiments on the new cubic Γ_3 systems PrT_2Al_{20}, where T corresponds to a transition metal such as Ti and V[23–26]. In these systems, the hybridization between the f-moments and the conduction ($c-$) electrons is found to be not only strong but tunable. The strong c-f hybridization is evident from a number of observations, including the Kondo-effect in the resistivity (i.e. $\rho(T) \propto -\ln T$)[23], a Kondo-resonance peak observed near the Fermi-energy[27], and a large hyperfine constant in the NMR measurements[28]. The tunability of the hybridization strength in PrT_2Al_{20} is demonstrated by both chemical and physical pressure measurements: the substitution of Ti by V enhances the Kondo-effect and induces an anomalous metallic behavior due to the hybridization. $PrTi_2Al_{20}$ exhibits a ferro-quadrupole ordering at $T_Q = 2$ K with a subsequent superconducting (SC) transition at $T_c = 0.2$ K[23,24]. While the SC effective mass of $PrTi_2Al_{20}$ is moderately enhanced under ambient pressure, i.e. $m^*/m_0 \sim 16$ (m_0 is the free electron mass), the application of pressure increases T_c up to 1 K and m^*/m_0 up to 110 at $P \sim 8$ GPa, while suppressing T_Q[25].This indicates that the pressure-induced heavy-fermion superconductivity emerges in the vicinity of a putative quadrupolar QCP.

Evidence for strong hybridization in PrV_2Al_{20} is fur-

ther provided by the recent discovery of heavy-fermion superconductivity at $T_c = 50$ mK with a large specific heat jump $\Delta C/T \sim 0.3$ J/mol K^2 below $T_Q = 0.6 - 0.7$ K under ambient pressure[26]. The effective mass of the quasiparticles participating into the superconducting condensate is found to be as large as 140 m_0, which is one order of magnitude larger than that of its Ti analog[24]. This result indicates that PrV_2Al_{20} should be located in the vicinity of a QCP associated *only* with multipole moments.

To realize such quantum criticality due to multipole moments, the magnetic field is another useful control parameter that couples quadratically with quadrupole moments, thus more weakly than with magnetic moments. The high-field phase diagram of PrV_2Al_{20} was investigated through specific-heat measurements under fields up to 9 T applied along all three main crystallographic orientations. Overall, the low-field phase boundaries for the [100], [110] and [111] directions are very similar to one another and nearly independent of $\mu_0 H$, as often observed in various quadrupolar ordered systems[20,23]. Moreover, high field magnetization measurements revealed a field induced first-order transition at $\mu_0 H \sim 11$ T for H||[100] which is most likely due to the switching of the quadrupole order parameter in the Γ_3 ground doublet[29].

Here, we report the discovery of field-tuned quantum criticality based solely on the quadrupolar (orbital) degrees of freedom at ambient pressure in PrV_2Al_{20}. We studied, through magneto-transport measurements, the magnetic phase diagram of PrV_2Al_{20} for H||[111]. We found unusual non-Fermi liquid behavior, i.e. $\rho = \rho_0 + AT^n$ with $n \leq 0.5$, a divergent quasiparticle effective mass and a large enhancement in the residual resistivity ρ_0 around the magnetic field-induced quantum-phase transition at the critical-field $\mu_0 H_c \sim 11$ T, where the quadrupolar transition temperature is suppressed to absolute zero. In addition, our observation of quantum oscillations reveal a heavy mass state with $m^*/m_0 > 10$ in the paraquadrupolar state beyond $\mu_0 H_c$, indicating nonmagnetic Kondo effect competing with the quadrupolar coupling as the origin of the pronounced quantum criticality observed over an extensive region of T and $\mu_0 H$. The experimental condition is described in detail in the supplemental material[30].

The temperature dependence of the resistivity $\rho(T)$ in both the low field ($\mu_0 H \leq 8$ T) and the high field ($\mu_0 H \geq 9.5$ T) regions, is presented in Figs. 1(a) and 1(b), respectively. Both the magnetic field and the electric currents were applied along the [111] direction. When the field is lower than 10 T, one observes a sudden decrease in $\rho(T)$ upon cooling due to the quadrupolar phase-transition. Correspondingly, a peak is observed in the T derivative of the resistivity at a low temperature T_Q which systematically changes with field, as shown in Fig. 1(c). On the other hand, the resistivity under fields surpassing 11 T shows such a smooth temperature dependence that the anomaly associated with the quadrupolar

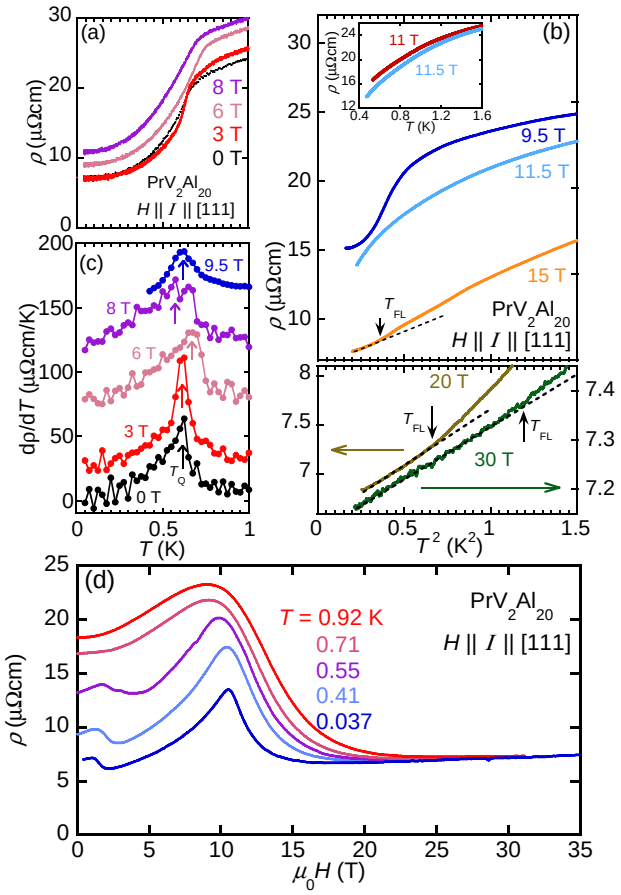

FIG. 1. (Color online) (a, b) Longitudinal resistivity ρ for PrV_2Al_{20} single-crystals as a function of temperature T under magnetic fields. The solid arrow indicates the characteristic temperature T_{FL} below which $\rho(T)$ exhibits a T^2 dependence (dashed line). (c) Derivative of the resistivity with respect to temperature $d\rho/dT$ and as function of T, for fields below 10 T. The data points are vertically shifted for clarity. The arrows indicate the quadrupolar transition temperature T_Q. (d) ρ as a function of $\mu_0 H$ ||[111] at various temperatures.

ordering no longer exists. Thus, a quantum phase transition between the low-field quadrupolar and high-field paraquadrupolar phases should be located at $\mu_0 H_c \sim 11$ T. Such a field-induced suppression of a quadrupolar phase was predicted for the PrT_2Al_{20} system using a mean-field theory based on a localized picture[31]. Previous magnetization measurements[29] for fields aligned along [111]-direction did not detect evidence for an ordered state in contrast to what is observed for fields aligned along the [100]-direction. This is consistent with our results.

Under a field of 11 T the resistivity displays a sublinear dependence on T, which contrasts markedly with the Fermi liquid behavior, i.e. $\rho \propto T^2$, shown in the inset of Fig. 1 (b). In contrast, for fields beyond 15 T the resistivity displays a super-linear or T^2-dependence

at the lowest temperatures as seen in Fig. 1 (b). A detailed analysis of the field and temperature dependence of ρ will be described below. Figure 1(d) displays the field dependence of the magnetoresistivity for $T < 1$ K. $\rho(H)$ exhibits a sharp peak at $\mu_0 H_c \sim 11$ T. In addition, below 10 T it displays a marked drop as the temperature is reduced below $T = 0.6$ K, due to the transition towards quadrupolar ordered state. If this peak resulted solely from thermal critical fluctuations associated with a finite temperature transition between the quadrupolar phase to the paraquadrupolar state, this peak would be expected to shift to lower fields with increasing T and eventually reach zero field near $T_Q \sim 0.6$ K. However in PrV_2Al_{20}, a pronounced peak is still observed at nearly the same field ~ 11 T at $T \sim 1$ K $>> T_Q$, indicating the development of quantum critical scattering at $\sim \mu_0 H_c$ and at much higher Ts than T_Q. In addition to the main peak at ~ 11 T, a small peak was observed below 2 T in the quadrupolar ordered state below 0.6 K. This may be associated with the change in the order parameters such as the lifting of the degeneracy between the O_0^2 and O_2^2 states[31].

To clearly illustrate the field-induced enhancement of the resistivity above T_Q, Fig. 2(a) shows a contour plot of ρ as a function of both T and $H \parallel [111]$. The change in color between blue and green at ~ 0.5 K found below 10 T follows the quadrupolar transition temperature T_Q (squares) determined by the temperature scans discussed above. This line of T_Q connects smoothly with the line depicting the peak position (circle) in the field dependence of the resistivity $\rho(H)$. These results indicate that the peak in the magnetoresistance at low temperatures corresponds to the quadrupolar phase boundary (solid line in Fig. 2(a)), which reaches the quantum critical point at $\mu_0 H_c \sim 11$ T.

Remarkably, the peak observed in $\rho(H)$ around 11 T survives up to ~ 1 K $> T_Q$ as discussed above, and this pronounced peak in $\rho(T, H)$ (red region in Fig. 2(a)), which is observed in the paraquadrupolar regime cannot be explained within a simple localized f-moment scenario. Figure 2 (b) shows $\rho(T)$ as a function of $T^{1/2}$ at $\mu_0 H = 11$ T near the quantum-critical field. $\rho(T)$ under $\mu_0 H = 11$ and 11.5 T shows a concave curvature, indicating that the exponent n in $\rho(T) = \rho_0 + AT^n$ is even smaller than 0.5. On the contrary, above 15 T, $\rho(T)$ exhibits a convex curvature indicating the emergence of Fermi liquid behavior at the lowest Ts, as shown in Fig. 1 (b). The characteristic temperature T_{FL} below which $\rho(T)$ displays FL-behavior or $\rho(T) = \rho_0 + AT^2$ increases with field (Fig. 2 (a)). Figure 2 (c) indicates the field dependence of $A^{-1/2}$ obtained from $\rho(T)$ above 15 T. Accordingly, upon approaching the quantum-critical field, the corresponding A values diverge, exceeding ~ 5 $\mu\Omega$cm/K^2. It can be fit to $\sqrt{A} = \sqrt{A_0}/(\mu_0 H - \mu_0 H_c^A)$ with $\sqrt{A_0} = 8.92$ $(\mu\Omega\text{cm T/K}^2)^{1/2}$, and $\mu_0 H_c^A = 10.5$ T (Fig. 2(c)). Significantly, $\mu_0 H_c^A$ is found to be consistent with the critical field ~ 11 T determined by the peak in $\rho(H)$. According to the Kadowaki-Woods relation, the

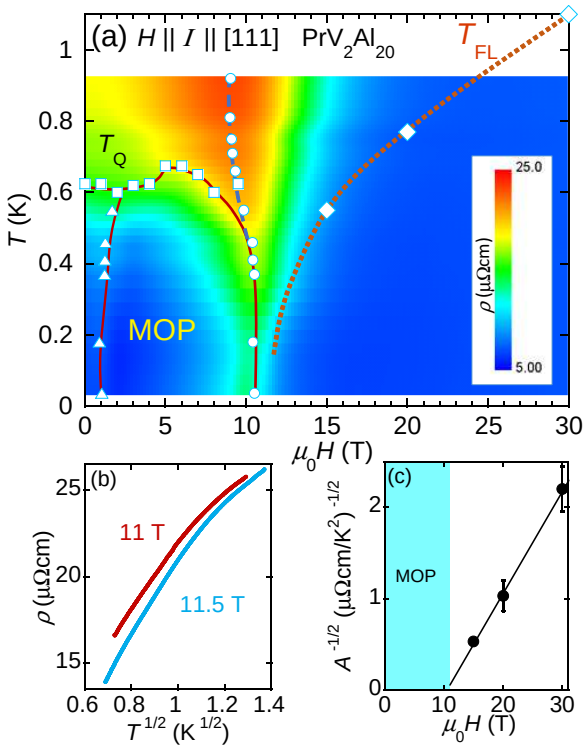

FIG. 2. (Color online) (a) Magnetic phase diagram of PrV_2Al_{20} for fields, and current I, parallel to the [111] direction. Color plot indicates the $\rho(T, H)$ values obtained from H scans under constant T. Circles indicate the peak position at $\mu_0 H_c \sim 11$ T, separating the low-field multipole ordering phase (MOP) and the paraquadrupolar state at high fields. Triangles represent small peaks observed in $\rho(H)$ for fields below 2 T. The solid line and broken line show the transition temperature/field of the multipole ordered phase and the peak position in $\rho(H)$, respectively. Squares and diamonds respectively indicate T_Q as determined from the peak in $d\rho(T)/dT$ and a characteristic temperature T_{FL} below which $\rho(T)$ follows the Fermi-liquid T^2 law. The dotted line is a guide to the eyes. (b) ρ as a function of $T^{1/2}$ under $\mu_0 H = 11$ and 11.5 T. (c) Field dependence of $A^{-1/2}$, where A is the T^2 coefficients in $\rho(T)$. The solid line is the fit to $\sqrt{A} = \sqrt{A_0}/(\mu_0 H - \mu_0 H_c)$.

critical enhancement in $A^{1/2}$ indicates the divergence of the effective mass upon approaching the QCP.

The sharp magnetoresistance peak at $\mu_0 H_c \sim 11$ T, which is observed even above T_Q, indicates a significant role for hybridization effects in the quantum criticality. In effect, at a pressure-induced quantum critical point, the enhancement in the residual resistivity has been reported and attributed to quantum critical fluctuations[2]. In Pr-based compounds with a Γ_3 ground doublet, such an enhancement in ρ_0 was also observed under zero field, especially above ~ 7 GPa in $PrTi_2Al_{20}$, which is accompanied by the suppression of the quadrupole-order[25]. T_c as well as the effective mass m^* also increase considerably above ~ 7 GPa, while T_Q starts to decrease, suggesting

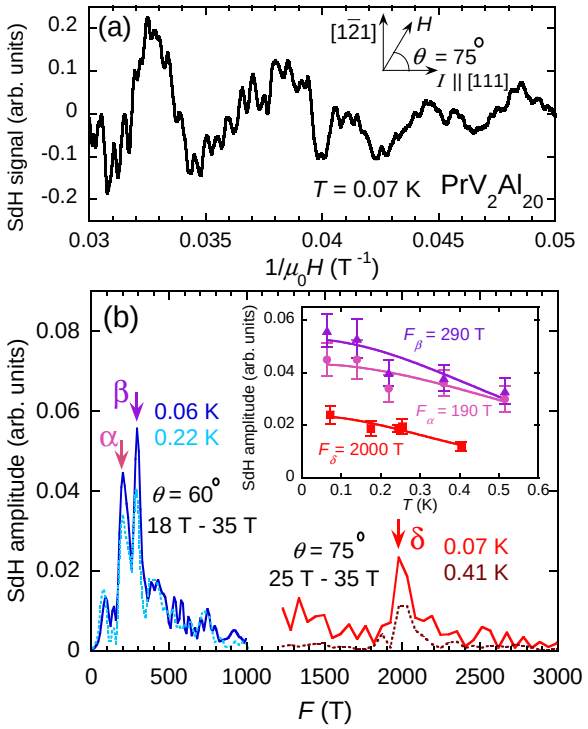

FIG. 3. (Color online) (a) Typical trace of the oscillatory signal due to the Shubnikov-de Haas effect (SdH), superimposed onto the $\rho(H)$ trace as a function of $\mu_0 H^{-1}$ for $T = 70$ mK and for an angle $\theta = 75°$ from [111] direction. (b) Fast Fourier transform (FFT) of the oscillatory signal for $\theta = 60°$ and at $T = 60$ and 220 mK, respectively. One observes two prominent peaks at $F_\alpha \sim 190$ T and $F_\beta \sim 290$ T. The same figure shows the FFT spectra for $\theta = 75°$ and $T = 70$ and 410 mK. For this orientation one detects a higher frequency $F_\delta \sim 2$ kT. Inset: Lifshitz-Kosevich fits of the SdH amplitude as a function of T from which we extract the corresponding effective masses $m^\star$.

the proximity to a putative quantum critical point[25]. In PrV_2Al_{20}, the similarly dramatic enhancement in both ρ_0 and in $m^* \sim A^{1/2}$ under magnetic field, coupled to the anomalous T-dependence of the resistivity at the critical field $\mu_0 H_c \simeq 11$ T, provides firm experimental evidence for field-induced quantum criticality based on the strong hybridization between the conduction electrons and the nonmagnetic quadrapolar / orbital degrees of freedom in the Γ_3 ground doublet. As discussed above, the resistivity follows $\rho = \rho_0 + AT^n$, with $n \leq 0.5$ at $\mu_0 H_c$, in sharp contrast to $n = 1$ and 1.5, which are usually observed around a QCP in Ce/Yb based heavy-fermion compounds with a ground Kramers doublet[9–13].

Finally, the high-quality of our single crystals allows us to observe the Shubnikov-de Haas (SdH) effect above the critical field. Figure 3(a) illustrates a representative trace of the oscillatory signal superimposed into $\rho(H)$ (after subtraction of a polynomial fit) at $T = 70$ mK as a function of inverse field $1/\mu_0 H$, under fields aligned at an angle $\theta = 75°$ away from the [111] direction and beyond the critical value required to suppress the quadrupolar state. The corresponding fast Fourier-transform spectra is shown in Fig. 3 (b) for two values of T, respectively at 60 mK (dark blue trace) and 220 mK (clear blue trace). One detects two main small frequencies $F_\alpha \sim 190$ T and $F_\beta \sim 290$ T. Figure 3 (b) also displays two other traces for H at an angle $\theta = 75°$, and at $T = 70$ mK (dark orange trace) and 410 mK (brown trace) respectively, revealing a higher frequency $F_\delta \sim 2$ kT.

An important piece of information is provided by the inset in Fig. 3 (b) which displays the amplitude of the FFT peaks as a function of T: solid lines are fits to the Lifshitz-Kosevich thermal damping term, i.e. $X/\sinh X$ with $X = 4\pi^3 k_B m^\star T/eH$ (where k_B is the Boltzmann constant, and e is the electron charge) from which we extract the effective mass $m^\star$ for each F. The resulting mass values are $m^\star_\alpha = (5.7 \pm 1.2)m_0$, $m^\star_\beta = (6.8 \pm 1.2)m_0$ and $m^\star_\delta = (10.6 \pm 1.2)m_0$, which are still moderately heavy, indicating the presence of the nonmagnetic Kondo effect based on the $c - f$ hybridization. This indicates that the nonmagnetic Kondo effect has a much higher energy scale than the CEF gap at the critical field[30]. Thus, the quantum-critical behavior unveiled here cannot be ascribed to an f-electron localization transition involving the suppression of the Kondo-effect at low fields. The charge carriers are so heavy as $m^* \sim 140\ m_0$ at zero-field, and still display moderately heavy masses at high fields. dHvA measurements were performed also in the isostructural compound $PrTi_2Al_{20}$ which displays ferro-quadrupole ordering below 2 K[32]. The effective masses extracted for the various Fermi surface sheets range between 0.52 and 0.82 $m^\star/m_0$. These values are considerably smaller than the masses, ranging from 5.7 to 10 $m^\star/m_0$, observed in PrV_2Al_{20}. This difference in effective masses is qualitatively consistent with much heavier masses for PrV_2Al_{20}, or $\sim 140\ m_0$, versus $\sim 16\ m_0$ for $PrTi_2Al_{20}$ as estimated from their superconducting transition under zero field. In contrast with the divergence found in the A coefficient as $\mu_0 H \rightarrow \mu_0 H_c$, we could not detect any evolution of the cyclotron masses upon approaching the QCP thus indicating that other, probably undetected, Fermi surface sheets are involved in the QC phenomenology displayed by PrV_2Al_{20}, and that the detected cyclotronic orbits remain oblivious to the quantum fluctuations associated with orbital degrees of freedom. The observation of the SdH signal paves the path to further clarifying its electronic structure and to understanding the strong screening effects leading to the quadrupolar quantum criticality involving the prominent non-Fermi liquid behavior observed in PrV_2Al_{20}.

ACKNOWLEDGMENTS

We thank Y. Matsumoto, T. Tomita, T. Sakakibara, K. Araki. Y. Uwatoko, K. Matsubayashi, J. Suzuki, K. Miyake, K. Hattori and H. Kusunose for useful discus-

sions. This work was partially supported by Grants-in-Aid (No. 25707030 and 25887015) from JSPS, and by PRESTO, JST, Japan, and by Program for Advancing Strategic International Networks to Accelerate the Circulation of Talented Researchers (No. R2604) from the Japanese Society for the Promotion of Science Y. S. is partially supported by ICAM. The NHMFL is supported by NSF through NSF-DMR-0084173 and the State of Florida. L. B. is supported by DOE-BES through award DE-SC0002613. This work was supported in part by NSF Grant No. PHYS-1066293 and we acknowledge the hospitality of the Aspen Center for Physics.

* simu@issp.u-tokyo.ac.jp
† satoru@issp.u-tokyo.ac.jp

[1] P. Monthoux, D. Pines, and G. G. Lonzarich, Nature **450**, 1177 (2007).
[2] H. V. Löhneysen, A. Rosch, M. Vojta, and P. Wölfle, Rev. Mod. Phys. **79**, 1015 (2007).
[3] P. Gegenwart, Q. Si, and F. Steglich, Nature Phys. **4**, 186 (2008).
[4] E. D. Bauer, N. A. Frederick, P.-C. Ho, V. S. Zapf, and M. B. Maple, Phys. Rev. B **65**, 100506 (2002).
[5] K. Miyake, H. Kohno, and H. Harima, J. Phys.: Condensed Matter **15**, L275 (2003).
[6] K. Hattori, J. Phys. Soc. Jpn. **79**, 114717 (2010).
[7] H. Kontani and S. Onari, Phys. Rev. Lett. **104**, 157001 (2010).
[8] Y. Yanagi, Y. Yamakawa, N. Adachi, and Y. Ono, J. Phys. Soc. Jpn. **79**, 123707 (2010).
[9] N. D. Mathur, F. M. Grosche, S. R. Julian, I. R. Walker, D. M. Freye, R. K. W. Haselwimmer, and G. G. Lonzarich, Nature **394**, 39 (1998).
[10] H. Hegger, C. Petrovic, E. G. Moshopoulou, M. F. Hundley, J. L. Sarrao, Z. Fisk, and J. D. Thompson, Phys. Rev. Lett. **84**, 4986 (2000).
[11] J. Paglione, M. A. Tanatar, D. G. Hawthorn, E. Boaknin, R. W. Hill, F. Ronning, M. Sutherland, L. Taillefer, C. Petrovic, and P. C. Canfield, Phys. Rev. Lett. **91**, 246405 (2003).
[12] P. Gegenwart, J. Custers, C. Geibel, K. Neumaier, T. Tayama, K. Tenya, O. Trovarelli, and F. Steglich, Phys. Rev. Lett. **89**, 056402 (2002).
[13] S. Nakatsuji, K. Kuga, Y. Machida, T. Tayama, T. Sakakibara, Y. Karaki, H. Ishimoto, S. Yonezawa, Y. Maeno, E. Pearson, G. G. Lonzarich, L. Balicas, H. Lee, and Z. Fisk, Nature Phys. **4**, 603 (2008).
[14] Y. Tokura and N. Nagaosa, Science **288**, 462 (2000).
[15] S. Nakatsuji, K. Kuga, K. Kimura, R. Satake, N. Katayama, E. Nishibori, H. Sawa, R. Ishii, M. Hagiwara, F. Bridges, T. U. Ito, W. Higemoto, Y. Karaki, M. Halim, A. A. Nugroho, J. A. Rodriguez-Rivera, M. A. Green, and C. Broholm, Science **336**, 559 (2012).
[16] P. Morin, D. Schmitt, and E. du Tremolet de Lacheisserie, J. Magn. Magn. Mater. **30**, 257 (1982).
[17] H. Suzuki, M. Kasaya, T. Miyazaki, Y. Nemoto, and T. Goto, J. Phys. Soc. Jpn. **66**, 2566 (1997).
[18] T. Onimaru, T. Sakakibara, N. Aso, H. Yoshizawa, H. S. Suzuki, and T. Takeuchi, Phys. Rev. Lett. **94**, 197201 (2005).
[19] T. Onimaru, K. T. Matsumoto, Y. F. Inoue, K. Umeo, Y. Saiga, Y. Matsushita, R. Tamura, K. Nishimoto, I. Ishii, T. Suzuki, and T. Takabatake, J. Phys. Soc. Jpn. **79**, 033704 (2010).
[20] T. Onimaru, K. T. Matsumoto, Y. F. Inoue, K. Umeo, T. Sakakibara, Y. Karaki, M. Kubota, and T. Takabatake, Phys. Rev. Lett. **106**, 177001 (2011).
[21] D. L. Cox, Phys. Rev. Lett. **59**, 1240 (1987).
[22] A. Yatskar, W. P. Beyermann, R. Movshovich, and P. C. Canfield, Phys. Rev. Lett. **77**, 3637 (1996).
[23] A. Sakai and S. Nakatsuji, J. Phys. Soc. Jpn. **80**, 063701 (2011).
[24] A. Sakai, K. Kuga, and S. Nakatsuji, J. Phys. Soc. Jpn. **81**, 083702 (2012).
[25] K. Matsubayashi, T. Tanaka, A. Sakai, S. Nakatsuji, Y. Kubo, and Y. Uwatoko, Phys. Rev. Lett. **109**, 187004 (2012).
[26] M. Tsujimoto, Y. Matsumoto, T. Tomita, A. Sakai, and S. Nakatsuji, Accepted for publication in Phys. Rev. Lett. (arXiv:1407.0866) (2014).
[27] M. Matsunami, M. Taguchi, A. Chainani, R. Eguchi, M. Oura, A. Sakai, S. Nakatsuji, and S. Shin, Phys. Rev. B **84**, 193101 (2011).
[28] Y. Tokunaga, H. Sakai, S. Kambe, A. Sakai, S. Nakatsuji, and H. Harima, Phys. Rev. B **88**, 085124 (2013).
[29] Y. Shimura, Y. Ohta, T. Sakakibara, A. Sakai, and S. Nakatsuji, J. Phys. Soc. Jpn. **82**, 043705 (2013).
[30] See Supplemental Material, which includes Refs. [33, 34, 35] at [URL will be inserted by publisher] for the experimental method and the analysis of the CEF under magnetic field.
[31] K. Hattori and H. Tsunetsugu, J. Phys. Soc. Jpn. **83**, 034709 (2014).
[32] S. Nagashima, T. Nishiwaki, A. Otani, M. Sakoda, E. Matsuoka, H. Harima, and H. Sugawara, JPS Conf. Proc. **3**, 011019 (2014).
[33] K. Lea, M. Leask, and W. Wolf, J. Phys. Chem. Solids **23**, 1381 (1962).
[34] K. Araki, Y. Shimura, N. Kase, T. Sakakibara, A. Sakai, and S. Nakatsuji, JPS Conf. Proc. **3**, 011093 (2014).
[35] Y. Aoki, T. Namiki, T. D. Matsuda, K. Abe, H. Sugawara, and H. Sato, Phys. Rev. B **65**, 064446 (2002).